NOTES 16.

STATIC AND DYNAMIC FORCED PERFORMANCE OF TILTING PAD BEARINGS: ANALYSIS INCLUDING PIVOT STIFFNESS

Dr. Luis San Andrés
Mast-Childs Professor
August 2010

SUMMARY

Work in progress – still a lot of be done

Introduction

Figure 1 shows a tilting pad journal bearing comprised of four pads. Each pad tilts about its pivot making a hydrodynamic film that generates a pressure reacting to the static load applied on the spinning journal. This type of bearing is typically installed to carry a static load on a pad (LOP) or a static load in between pads (LBP). Commercial tilting pad bearings have various pivot designs such as rocker pivots (line contact), spherical pivots (point contact) and flexure supported pivots.

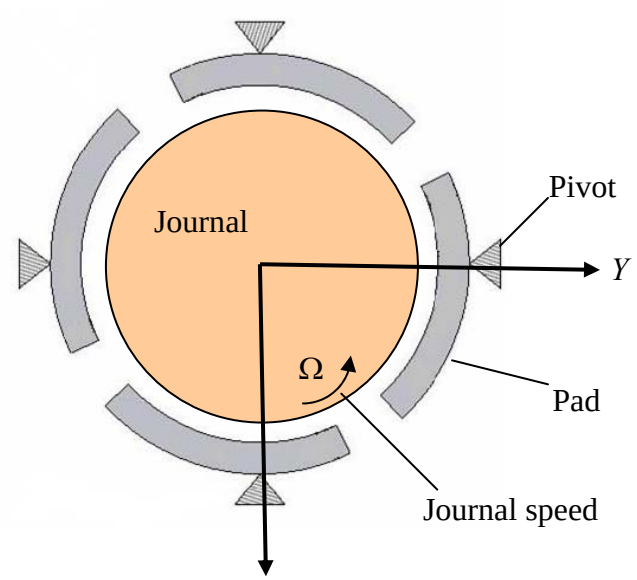

Figure 1. Schematic view of a four pad tilting pad bearing, Ref. [1]

Accurate prediction of tilting pad bearing forces and force coefficients is essential to design and predict the dynamic performance of rotor-bearing systems. Parameters affecting tilting pad bearing force coefficients include elastic deformation of the bearing pads and pivots, thermal effects affecting the lubricant viscosity and film clearance, etc. [2,3].

ANALYSIS

Rocker and spherical pivots in tilting pad allow nearly frictionless pad rotation. An ideal rocker TPB, shown in Fig. 3(a), allows the pad to roll without slipping around a cylindrical pivot inside the curvature of the bearing. A spherical TPB, seen in Fig. 3(b), allows the pad to rotate about a spherical pivot fixed to the inside curvature of the bearing.

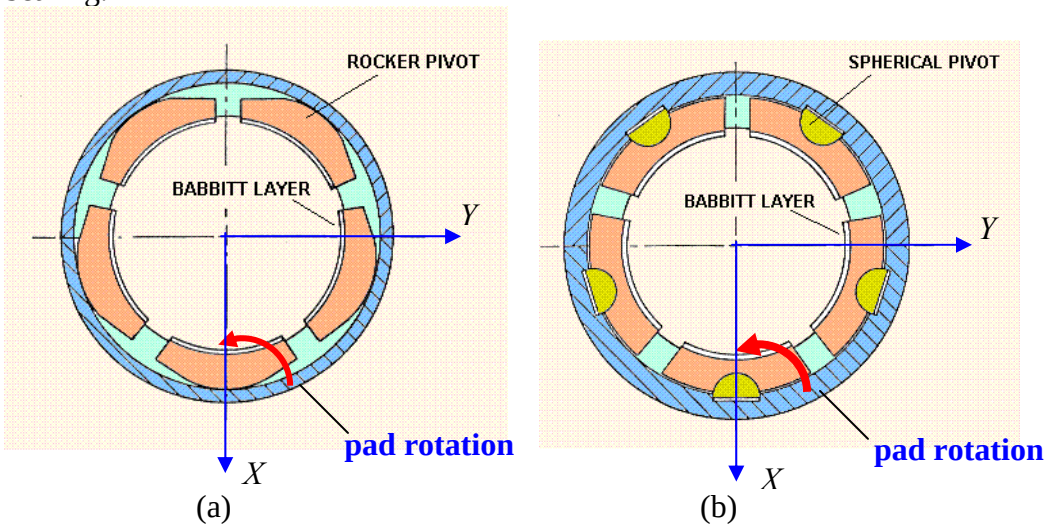

Figure 3. Rocker pivot (a) and spherical pivot (b) in a tilting pad journal bearing [15]

The flexure pivot TBP, depicted in Fig. 4, is a modern advancement in TBP designs. It is a two piece configuration that uses electron discharge machining to manufacture the pad, connected by a flexure thin web to the bearing housing. This design eliminates tolerance stack ups that usually occur during manufacturing and assembly, pivot wear, and unloaded pad flutter problems which occur in conventional tilting pad bearings [16].

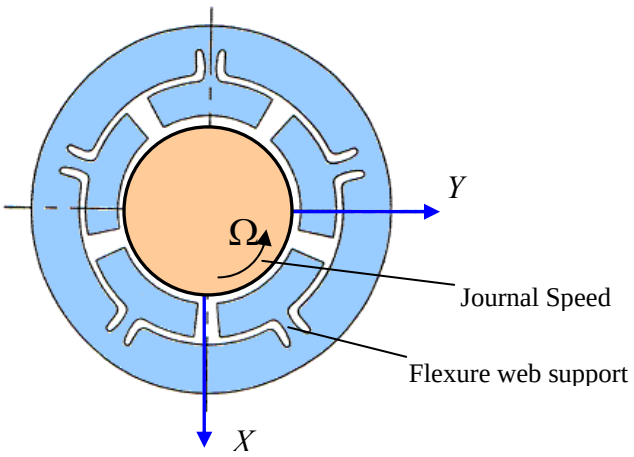

Figure 4. Schematic view of flexure pivot TPB [13]

As seen in Fig. 5, pivot flexibility makes the pad to displace along the radial (ξ) and transverse (η) directions. The pad also tilts or rotates with angle (δ).

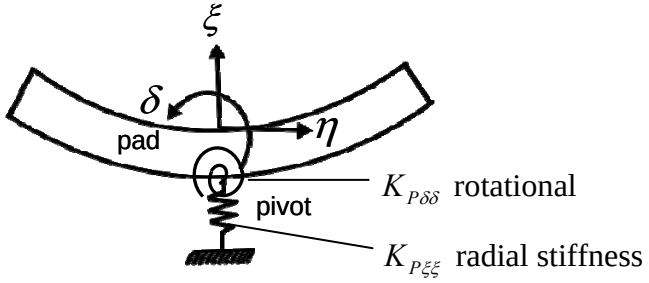

Figure 5. Displacement coordinates in a tilting pad with idealized depiction of pivot stiffnesses

Coordinate system and film thickness

Figure 6 shows the geometry and coordinate system for a tilting pad journal bearing. A local coordinate is placed on the bearing surface with the $\{x\}$ axis in the circumferential direction and the $\{z\}$ axis in the axial (in plane) direction. Inertial axes $\{X,Y,Z\}$ have origin at the bearing center. e_X, e_Y represent the journal center displacements along the X,Y axes. The position of a tilting-pad is referenced to the angular coordinate $\theta = \frac{x}{R}$, with Θ_l as the pad leading edge angle, Θ_t as the pad trailing edge angle, and Θ_P as the pad pivot point angle. $\left(\delta^k, \xi^k, \eta^k\right)$ denote the k^{th} pad rotation and radial and transverse displacements; $k = 1,...N_{pad}$.

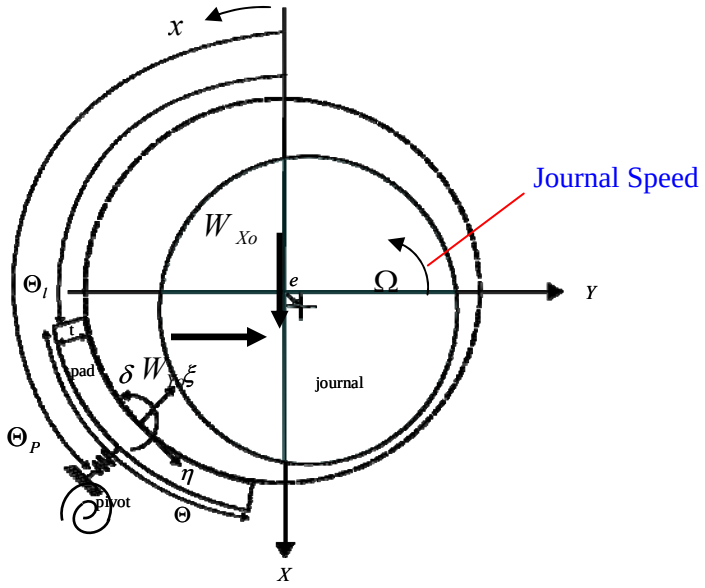

Figure 6. Geometry and nomenclature for a tilting pad with flexible pivot

The fluid film thickness in the k^{th} pad is [17],

$$h^k = C_p + e_X \cos(\theta) + e_Y \sin(\theta) + (\xi^k - r_p)\cos(\theta - \Theta_p) + (\eta^k - R\delta^k)\sin(\theta - \Theta_p) \quad (1)$$

where C_p is the pad machined radial clearance, and $r_p = C_p - C_m$ is the pad preload with C_m as the bearing assembled clearance. Presently, for simplicity, a bearing pad is assumed rigid.

Journal motion perturbation analysis

The bearing supports a static load with components $\{W_{Xo}, W_{Yo}\}$. At speed Ω, the static load determines operation with the journal at its static equilibrium position (e_{Xo}, e_{Yo}). At equilibrium, in the k^{th} pad, the ensuing film thickness is $\{h_o^k\}$ generating a hydrodynamic pressure field $\{P_o^k\}$. Each pad undergoes a rotation δ_o^k and the pivot deflects or displaces $\left(\xi_o^k, \eta_o^k\right)$.

Consider small amplitude journal center motions ($\Delta e_X, \Delta e_Y$) of frequency ω about the static equilibrium point (e_{Xo}, e_{Yo}). Hence, the journal center position, pad rotation angle and pivot displacements are

$$e_X(t) = e_{Xo} + \Delta e_X e^{i\omega t}, \qquad e_Y(t) = e_{Yo} + \Delta e_Y e^{i\omega t},$$

$$\delta^k(t) = \delta_o^k + \Delta\delta^k e^{i\omega t}, \quad \xi^k(t) = \xi_o^k + \Delta\xi^k e^{i\omega t}, \quad \eta^k(t) = \eta_o^k + \Delta\eta^k e^{i\omega t}, \quad k = 1,..N_{pad} \quad (2)$$

The pads film thicknesses and hydrodynamic fluid film pressures are also the superposition of equilibrium (zeroth order) and perturbed (first order) fields, i.e.,

$$h^k = h_o^k + \Delta h^k e^{i\omega t} \quad (3)$$

$$P^k = P_o^k + \Delta P^k e^{i\omega t} \quad (4)$$

where $\Delta h^k = \Delta e_X \cos\theta + \Delta e_Y \sin\theta + \Delta\xi^k \cos(\theta - \Theta_p^k) + (\Delta\eta^k - R\Delta\delta^k)\sin(\theta - \Theta_p^k)$ (5)

and $$\Delta P^k = P_X^k \Delta e_X + P_Y^k \Delta e_Y + P_\delta^k \Delta\delta^k + P_\xi^k \Delta\xi^k + P_\eta^k \Delta\eta^k \quad , \; k = 1,..N_{pad} \quad (6)$$

Pad fluid film forces and pad moment

Fluid film reaction forces acting on the rotating journal are a result of the hydrodynamic pressure fields,

$$\begin{bmatrix} F_X^k \\ F_X^k \end{bmatrix} = \int_{-L_L}^{-L_R} \int_{\Theta_l^k}^{\Theta_l^k + \Theta^k} P^k \begin{bmatrix} \cos\theta \\ \sin\theta \end{bmatrix} R d\theta^k dz \qquad k = 1,..N_{pad} \quad (7)$$

The fluid film moment acting on a tilting pad is a result of these forces. i.e.

$$M^k = -(R+t)[F_Y^k \cos\Theta_P - F_X^k \sin\Theta_P] = -R_p F_\eta^k \qquad k = 1,..N_{pad} \qquad (8)$$

where R is the pad radius and t is the pad thickness. See Appendix A for details on the derivation of Eq. (8)

The fluid forces and moment are decomposed into static and dynamic parts, i.e.

$$F_X^k = F_{Xo}^k + \Delta F_X^k e^{i\omega t} = F_{Xo}^k - \{Z_{XX}\Delta e_X + Z_{XY}\Delta e_Y + Z_{X\delta}\Delta\delta + Z_{X\xi}\Delta\xi + Z_{X\eta}\Delta\eta\}^k e^{i\omega t}$$

$$F_Y^k = F_{Yo}^k + \Delta F_Y^k e^{i\omega t} = F_{Yo}^k - \{Z_{YX}\Delta e_X + Z_{YY}\Delta e_Y + Z_{Y\delta}\Delta\delta + Z_{Y\xi}\Delta\xi + Z_{Y\eta}\Delta\eta\}^k e^{i\omega t} \qquad (9)$$

$$M^k = M_o^k + \Delta M^k e^{i\omega t} = M_o^k - \{Z_{\delta X}\Delta e_X + Z_{\delta Y}\Delta e_Y + Z_{\delta\delta}\Delta\delta + Z_{\delta\xi}\Delta\xi + Z_{\delta\eta}\Delta\eta\}^k e^{i\omega t}$$

$$k = 1,..N_{pad}$$

where the zeroth order fluid film forces (F_{Xo}^k, F_{Yo}^k), and pad moment (M_o^k) are:

$$\begin{bmatrix} F_{Xo}^k \\ F_{Yo}^k \end{bmatrix} = \int_{-L_L}^{-L_R}\int_{\Theta_{lk}}^{\Theta_{lk}+\Theta_k} -P_o^k \begin{bmatrix} \cos\theta \\ \sin\theta \end{bmatrix} R d\theta dz \qquad (10)$$

$$M_o^k = R_p\{F_{Xo}^k \sin(\Theta_p^k) - F_{Yo}^k \cos(\Theta_p^k)\} = -R_p F_{\eta o}^k \qquad k = 1,..N_{pad} \qquad (11)$$

In Eq. (9), $\left(Z_{\alpha\beta}\right)^k$ are fluid film impedance coefficients whose real part and imaginary part give stiffness and damping coefficients, respectively. For the force impedances due to journal center displacements (Δe_X, Δe_Y),

$$Z_{\alpha\beta}^k = K_{\alpha\beta}^k + i\omega C_{\alpha\beta}^k = \int_{-L_L}^{-L_R}\int_{\Theta_l^k}^{\Theta_l^k+\Theta^k} P_\beta^k h_\alpha R d\theta^k dz \qquad \alpha,\beta = X,Y \qquad (12)$$

where $h_X = \cos(\theta)$ and $h_Y = \sin(\theta)$.

San Andrés [2] carries out the substitution of Eqs. (3-4) into the Reynolds equation to obtain a nonlinear PDE for the equilibrium pressure $\{P_o\}$ and linear PDEs for the first order fields. **In Ref. [2], San Andrés shows that the first order pressure fields satisfy homogeneous boundary conditions**. Hence, the dynamic pressure fields due to angular (δ^k), radial (ξ^k), and transverse (η^k) motions of the k^{th} pad satisfy the following relationships

$$P_\delta^k = R_p\{\sin(\Theta_p^k)P_X^k - \cos(\Theta_p^k)P_Y^k\}$$

$$P_\xi^k = \cos(\Theta_p^k)P_X^k + \sin(\Theta_p^k)P_Y^k \qquad k = 1,..N_{pad} \qquad (13)$$

$$P_\eta^k = -\sin(\Theta_p^k) P_X^k + \cos(\Theta_p^k) P_Y^k$$

A major simplification follows from Eq. (13), i.e., ($P_\delta^k, P_\xi^k, P_\eta^k$) are linear combinations of (P_X^k, P_Y^k). Thus impedance coefficients due to pad rotation, and pad-pivot radial and transverse displacements ($Z_{\alpha\beta}^k, \alpha,\beta = \delta,\xi,\eta$) are readily expressed as functions of the force-displacement impedances ($Z_{\alpha\beta}^k$, $\alpha,\beta = X,Y$). Reference [18] details the formulae for each fluid film impedance coefficient.

Pad Equilibrium Equations and Pad Equations of Motion

The sum of the pads fluid film reaction forces must balance the external load (W_X, W_Y) applied on the journal. The external forces add a static (equilibrium) (W_{Xo}, W_{Yo}) load to a dynamic part $(\Delta W_X, \Delta W_Y)e^{i\omega t}$.

$$W_X = W_{Xo} + \Delta W_X e^{i\omega t} = -\sum_{k=1}^{N_{pad}} F_X^k, \qquad W_Y = W_{Yo} + \Delta W_Y e^{i\omega t} = -\sum_{k=1}^{N_{pad}} F_Y^k \tag{14}$$

The equations of motion for the k^{th} pad are

$$\left[M_{pad}^k\right]\begin{Bmatrix}\Delta\ddot{\delta}^k\\ \Delta\ddot{\xi}^k\\ \Delta\ddot{\eta}^k\end{Bmatrix} = \begin{Bmatrix}M_P^k\\ F_{P\xi}^k\\ F_{P\eta}^k\end{Bmatrix} + \begin{Bmatrix}M^k\\ F_\xi^k\\ F_\eta^k\end{Bmatrix} \tag{15}$$

where M_P^k, $F_{P\xi}^k$, $F_{P\eta}^k$ are the pad pivot reaction moment and forces, and M^k, F_ξ^k, F_η^k are the fluid film forces acting on the k^{th} pad.

The pad mass matrix is

$$\left[M_{pad}^k\right] = \begin{bmatrix} I_P^k & m^k b^k & -m^k c^k \\ m^k b^k & m^k & 0 \\ -m^k c^k & 0 & m^k \end{bmatrix} \tag{16}$$

with *b* and *c* as the radial and transverse distances from the pad center of mass to the pad pivot, respectively. m^k and I_P^k are the pad mass and mass moment of inertia about the pad pivot. $I_P^k = I_G^k + m^k(c^2 + b^2)$, where I_G^k is the pad moment of inertia about its center of mass. See Appendix A for details on the derivation of Eq. (16)

The hydrodynamic pressure field determines the fluid film forces and moment acting on a pad. The pressure fields are obtained from solution of the fluid flow equations, either the Reynolds equation or bulk-flow equations. See Notes 7 and Notes 10 for details on the equations and the method of solution.

Evaluation of pivot nonlinear stiffness

The pivot stiffness is, in general, a nonlinear function of the applied (fluid film) load acting on a pad. Consider, as sketched in Figure 7, a typical radial force $F_{P\xi}$ versus pivot nonlinear radial deflection (ξ).

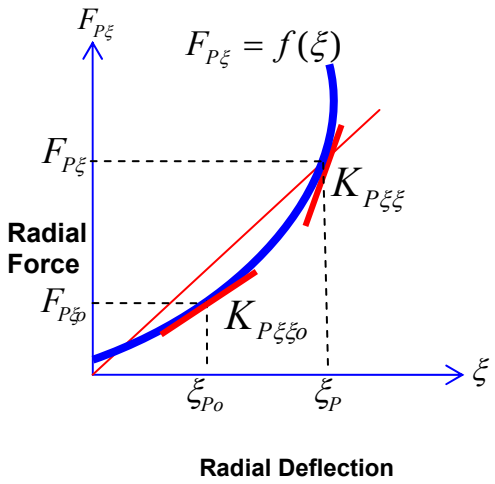

Figure 7. Typical force versus pivot (nonlinear) radial deflection

The local pivot stiffness is the slope of the load versus displacement curve, i.e.,

$$K_{P\xi\xi} = \frac{\partial F_{P\xi}}{\partial \xi_P} \tag{17}$$

The assumption of small amplitude motions about an equilibrium position allows the pivot reaction radial force to be expressed as

$$F_{P\xi} = F_{P\xi o} + K_{P\xi\xi o}\Delta\xi_P \tag{18}$$

where $F_{P\xi o} = f(\xi_{Po})$ is the static load on the pivot, and $K_{P\xi\xi o}\Delta\xi_P$ is the force due to radial displacement ($\Delta\xi$) of the pad.

The analysis of tilting pad bearings typically assumes either an **ideal point contact** or an **ideal line contact,** along with a negligible resistance to pad rotation [7]. The prediction of pivot stiffness in Ref. [7] is based upon Hertzian contact stress formulas in Ref. [11]. Ref. [7] details stiffness equations for a spherical pivot (point contact) and cylindrical pivot (line contact). Assuming the material properties of the pad pivot and its contact housing are the same, Kirk and Reedy [7] state the following pivot stiffness equations for physical parameters in US units:

Spherical pivot (point contact model)

$$K_{P\xi\xi} = (0.968)\sqrt[3]{\frac{E^2 D_H D_P F_{Po}}{D_H - D_P}} \tag{19}$$

Cylindrical (rocker) pivot (line contact model)

$$K_{P\xi\xi} = \frac{\pi EL}{2(1-\nu^2)\left[-\frac{1}{3} + \ln\left[\frac{(D_H - D_P)4EL}{2.15^2 F_{Po}}\right]\right]} \tag{20}$$

Above E and ν are the pivot material Young Modulus and Poisson ratio, respectively. D_H and D_P are the pivot housing diameter and pivot diameter, respectively. F_{Po} is the applied load on the pivot.

For an idealized flexure pivot pad bearing, Chen [9] treats the pad as a lumped inertia at the free end of a cantilever beam, see Fig. 8.

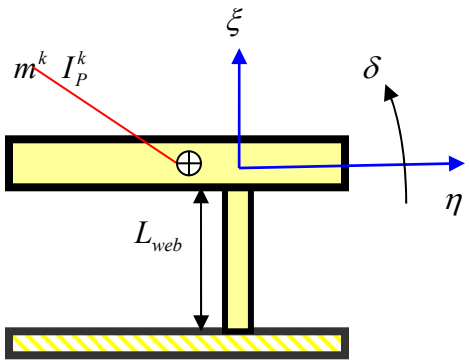

Figure 8: Cantilever beam model of a tilting pad with flexural web

The web deforms radially (ξ) and transversely (η) and the pad rotates with angular dispalcement (δ). The flexure pivot stiffness matrix is written as

$$[K_{pivot}] = \begin{bmatrix} K_{P\delta\delta} & 0 & K_{P\delta\eta} \\ 0 & K_{P\xi\xi} & 0 \\ K_{P\eta\delta} & 0 & K_{P\eta\eta} \end{bmatrix} \tag{21}$$

where [9]

$$K_{P\delta\delta} = \left(\frac{4EI}{L_{web}} - \frac{2F_{Po}L_{web}}{15}\right) \tag{22}$$

$$K_{P\delta\eta} = K_{P\eta\delta} = \left(\frac{-6EI}{L_{web}^2} - \frac{F_{Po}}{10}\right) \tag{23}$$

$$K_{P\xi\xi} = \left(\frac{AE}{L_{web}}\right) \tag{24}$$

$$K_{P\eta\eta} = \left(\frac{12EI}{L_{web}^3} - \frac{6F_{Po}}{5L_{web}} \right) \tag{25}$$

Above A, L_{web}, I, and E are the web cross sectional area, length of the flexure web, web area moment of inertia, and web modulus of elasticity, respectively. F_{Po} is the load passing through the support thin web. The equations above show the flexure stiffness coefficients are nonlinear.

Bearing rotordynamic force coefficients

Tilting pad bearing force coefficients are determined at the journal static equilibrium position and for a particular excitation frequency (ω), usually synchronous ($\omega = \Omega$), or subsynchronous ($\omega < \Omega$).

The journal center displaces along the $\{X, Y\}$ axes = two degrees of freedom (DOF). Each pad, on the other hand, has one rotation and two deflections, $(\delta, \xi, \eta)^k$ = three DOF. The total number of DOF in the bearing = 2 + 3 N_{pads}. Hence, the motion of the journal combined with those of the pads is complicated.

A simplification follows by assuming the pads move with the same frequency as the journal whirl frequency (ω). Substitution of Eq. (9) into Eq. (15) leads to the frequency reduced impedance coefficients [17]

$$[Z]_R = \begin{bmatrix} Z_{XX_R} & Z_{XY_R} \\ Z_{YX_R} & Z_{YY_R} \end{bmatrix} = [K]_R + i\omega[C]_R = \sum_{k=1}^{N_{pad}} [Z_{XY}^k] - [Z_a^k][Z_{P+f}^k]^{-1}[Z_b^k] \tag{26}$$

where

$$[Z_{XY}^k] = \begin{bmatrix} Z_{XX} & Z_{XY} \\ Z_{YX} & Z_{YY} \end{bmatrix}^k, \quad [Z_a^k] = \begin{bmatrix} Z_{X\delta} & Z_{X\xi} & Z_{X\eta} \\ Z_{Y\delta} & Z_{Y\xi} & Z_{Y\eta} \end{bmatrix}^k, \quad [Z_b] = \begin{bmatrix} Z_{\delta X} & Z_{\delta Y} \\ Z_{\xi X} & Z_{\xi Y} \\ Z_{\eta X} & Z_{\eta Y} \end{bmatrix}^k \tag{27}$$

and

$$[Z_{P+f}^k] = [K_{pivot}^k] + i\omega[C_{pivot}^k] + [Z_c^k] - \omega^2[M_{mass}^k], \quad [Z_c^k] = \begin{bmatrix} Z_{\delta\delta} & Z_{\delta\xi} & Z_{\delta\eta} \\ Z_{\xi\delta} & Z_{\xi\xi} & Z_{\xi\eta} \\ Z_{\eta\delta} & Z_{\eta\xi} & Z_{\eta\eta} \end{bmatrix}^k \tag{28}$$

where

$$[K_{pivot}^k] = \begin{bmatrix} K_{P\delta\delta} & 0 & K_{P\delta\eta} \\ 0 & K_{P\xi\xi} & 0 \\ K_{P\eta\delta} & 0 & K_{P\eta\eta} \end{bmatrix}^k, \quad [C_{pivot}^k] = \begin{bmatrix} C_{P\delta\delta} & 0 & C_{P\delta\eta} \\ 0 & C_{P\xi\xi} & 0 \\ C_{P\eta\delta} & 0 & C_{P\eta\eta} \end{bmatrix}^k \tag{29}$$

The frequency reduced stiffness and damping coefficient matrices are $[K]_R$ and $[C]_R$, respectively. The pivot stiffness matrix $[K^k_{pivot}]$ for the k^{th} pad of a flexure tilting pad bearing is found according to Eq. (21).

Under ideal operating conditions, the pads of a spherical or rocking tilting pad bearing will only deflect radially. Therefore, the matrix $[K^k_{pivot}]$ will contain an entry for the radial stiffness $(K_{P\xi\xi})$ only. For simplicity and absence of empirical data, pivot damping $[C^k_{pivot}]$ coefficients are negligible.

Iterative method for finding the static equilibrium position

The applied static load (W_{Xo}, W_{Yo}) determines the journal static equilibrium position (e_{Xo}, e_{Yo}). The analysis must calculate this operating eccentricity along with the static deflections and rotation for each pad.

$$W_{Xo} + \sum_{k=1}^{N_{pads}} F^k_{X_0} = 0; \quad W_{Yo} + \sum_{k=1}^{N_{pads}} F^k_{Y_0} = 0 \tag{30}$$

On each pad, the pivot reaction moment and forces must equal the pad fluid film moment and forces. From Eq. (15)

$$\begin{Bmatrix} M^k_{Po} \\ F^k_{P\xi o} \\ F^k_{P\eta o} \end{Bmatrix} + \begin{Bmatrix} M^k_{o} \\ F^k_{\xi o} \\ F^k_{\eta o} \end{Bmatrix} = 0 \tag{31}$$

A Newton-Raphson iterative procedure is devised to simultaneously satisfy the moment and forces balance of each pad as well as the static load condition on the journal. During the n^{th} iteration, Eq. (31) may not be satisfied, i.e.,

$$\begin{Bmatrix} M^k_{P} \\ F^k_{P\xi} \\ F^k_{P\eta} \end{Bmatrix}^n + \begin{Bmatrix} M^k \\ F^k_{\xi} \\ F^k_{\eta} \end{Bmatrix}^n = \left\{r^k\right\}^n \neq 0 \tag{32}$$

In order for the residual vector $\left\{r^k\right\}^n \rightarrow \{0\}$, pad displacements are incremented such that in the next iteration

$$\begin{Bmatrix} \delta^k \\ \xi^k \\ \eta^k \end{Bmatrix}^{n+1} = \begin{Bmatrix} \delta^k \\ \xi^k \\ \eta^k \end{Bmatrix}^n + \begin{Bmatrix} \overline{\Delta}\delta^k \\ \overline{\Delta}\xi^k \\ \overline{\Delta}\eta^k \end{Bmatrix}$$

Assuming that the displacement increments $\left\{\overline{\Delta}\delta^k \quad \overline{\Delta}\xi^k \quad \overline{\Delta}\eta^k\right\}^T$ are small, Eq. (31) is rewritten as

$$\begin{Bmatrix} M_P^k \\ F_{P\xi}^k \\ F_{P\eta}^k \end{Bmatrix} + \left[K_{pivot}^k\right] \begin{Bmatrix} \overline{\Delta}\delta^k \\ \overline{\Delta}\xi^k \\ \overline{\Delta}\eta^k \end{Bmatrix} + \begin{Bmatrix} M^k \\ F_\xi^k \\ F_\eta^k \end{Bmatrix} + \left[K_c^k\right] \begin{Bmatrix} \overline{\Delta}\delta^k \\ \overline{\Delta}\xi^k \\ \overline{\Delta}\eta^k \end{Bmatrix} = 0 \tag{33}$$

where $[K_c^k]$, the real part of $[Z_c^k]$, represents the static fluid film stiffnesses due to pad rotation and translations. Thus, the pad displacement vector is updated incrementally using the following:

$$\begin{Bmatrix} \overline{\Delta}\delta^k \\ \overline{\Delta}\xi^k \\ \overline{\Delta}\eta^k \end{Bmatrix} = -\left(\left[K_{pivot}^k\right] + \left[K_c^k\right]\right)^{-1} \begin{Bmatrix} M_P^k + M^k \\ F_{P\xi}^k + F_\xi^k \\ F_{P\eta}^k + F_\eta^k \end{Bmatrix}^n \tag{34}$$

In the process above, the journal position (e_{Xo}, e_{Yo}) remains invariant while the iterative method balances the static forces on each pad.

In order to balance the static load, i.e. $(W_o + F_o)_{X,Y} = 0$, a similar Newton-Raphson procedure is used to estimate improved journal eccentricity displacements, $\left\{e_{X,Y}^{n+1} = e_{X,Y}^n + \overline{\Delta}e_{X,Y}\right\}$, where

$$\begin{Bmatrix} \overline{\Delta}e_X \\ \overline{\Delta}e_Y \end{Bmatrix} = \left[[K]_R^n\right]^{-1} \begin{Bmatrix} \overline{\delta}W_X \\ \overline{\delta}W_Y \end{Bmatrix}^n \tag{35}$$

with $\begin{Bmatrix} \overline{\delta}W_X \\ \overline{\delta}W_Y \end{Bmatrix}^n$ as the residual vector of static forces and

$$[K]_R^n = \sum_{k=1}^{N_{pad}} \left([K_{XY}^k] - [K_a^k][K_{P+f}^k]^{-1}[K_b^k]\right)^n \tag{35}$$

as the matrix of reduced (bearing) **static stiffness coefficients**. Note that for the static case $\omega = 0$, the impedances $[Z_a^k]$, $[Z_{P+f}^k]$, and $[Z_b^k]$ have no imaginary part. Hence, $[K_a^k] = [Z_a^k]$, $[K_{P+f}^k] = [Z_{P+f}^k]$, and $[K_b^k] = [Z_b^k]$.

Comparison between predicted static and dynamic coefficients and Ref. [14] test measurements.

Figure 9 depicts a schematic view of a five pad, rocker back, TPB tested by Carter and Childs [14]. Bearing force coefficients were experimentally obtained for shaft speeds from 4k-12k rpm and static loads from 0-19.5 kN.

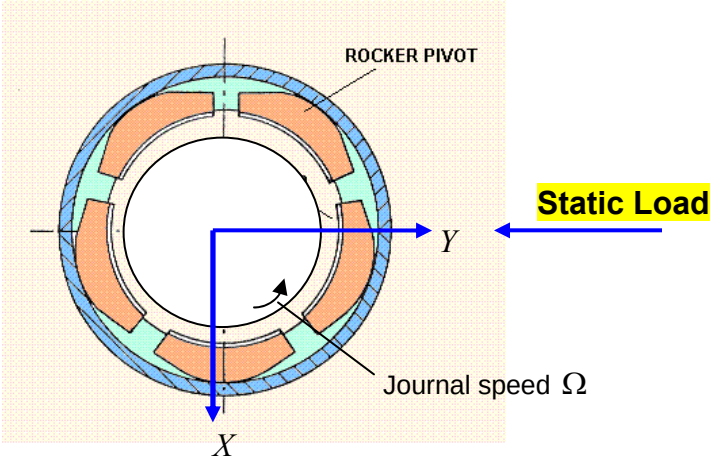

Figure 9: Five pad tilting pad bearing, Ref. [14]

Mineral oil (Mobil DTE) ISO VG32 lubricated the bearing. The lubricant inlet supply pressure and temperature are 1.55 bar (gauge) and 43° C, respectively. The load applied to the bearing is along the -*Y* direction. Table 1 details the bearing geometry and fluid properties.

Table 1: Test bearing geometry and operating conditions, Ref. [14]

Rotor diameter, D	101.587 mm
Pad axial length, L	60.32 mm
Pad number and arc length	5 (57.87°)
Pivot offset	60%
Loaded radial pad clearance, C_p	110.5 mm
Loaded radial bearing clearance, C_b	79.2 mm
Pad preload, $r_p = 1 - \dfrac{C_b}{C_p}$	0.283
Pad mass, m_p	1.0375 kg
Pad mass moment of inertia (at pivot), I_p	0.000449 kg-m^2
Fluid Properties, Ref. [19]	**Mobile DTE ISO VG32**
Viscosity @ 40° C	31 cSt
Viscosity @ 100° C	5.5 cSt
Density @ 15°C	850 kg/m^3
Specific heat	1951 J/(kg-K)

For load-between-pad configuration (LBP), Carter and Childs [14] present nonsynchronous force coefficients versus load. Figure 10 shows Ref. [14] predicted and experimental direct stiffnesses for a journal speed of 4 krpm. Experimental direct stiffness K_{YY} is over predicted by ~28% for a static load of 14.8 kN.

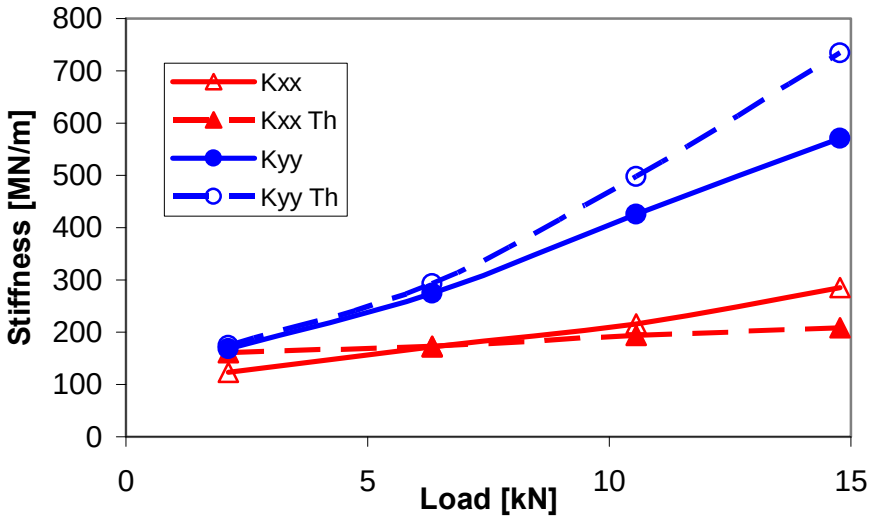

Figure 10: Predicted and experimental direct stiffness for operation shaft speed of 4 kprm, Ref. [14]

The experimental direct stiffness K_{XX} is over predicted at low loads (0-6 kN), but is under predicted at high loads (7-14.8 kN). The tilting pad bearing model assumes the pivot to be rigid, thus, when a flexible pivot is implemented into the model, the predicted direct stiffnesses will decreases.

Pad rocker pivot

The rocker pivot deflection equation as a function of load is given according to Kirk and Reedy [7]. Figure 11 shows rocker pivot deflection as a function of load.

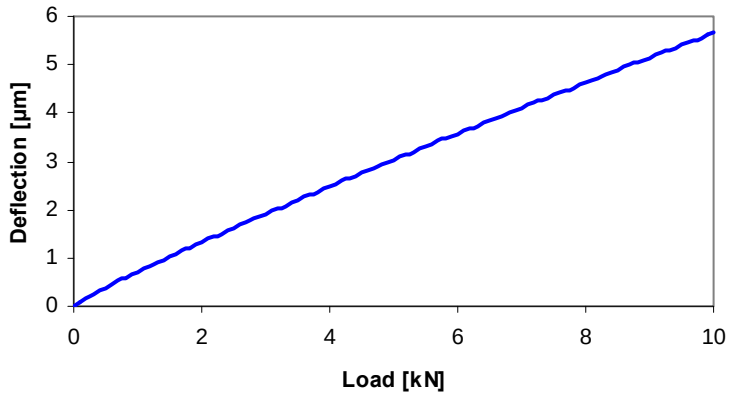

Figure 11: Rocker pivot deflection versus load

Rocker pivots usually cover the full axial length of the bearing pad, and thus are generally stiffer than spherical pivots.

Journal eccentricity and static stiffness coefficient predictions are predicted at a journal speed of 4,000 rpm. Figure 12 shows the predicted direct static force coefficients versus static load given a flexible rocker pivot and a rigid pivot for an isothermal flow case. The direct static stiffnesses decrease for a flexible pivot, the difference amounting to a large percentage, ~ 33%.

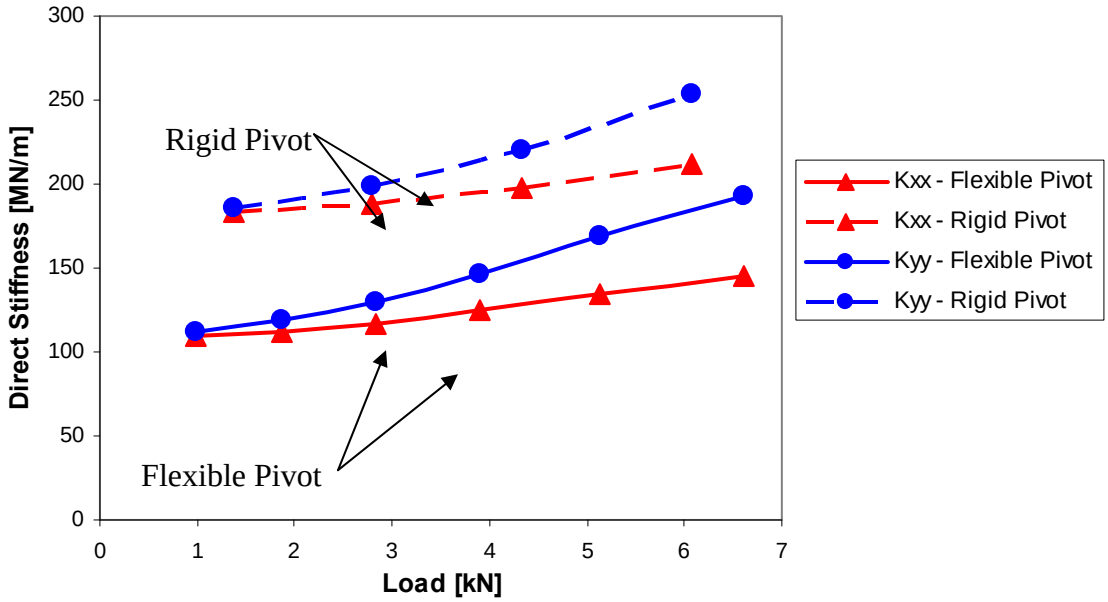

Figure 12: Predicted static direct stiffnesses versus static load

Figure 13 shows the predicted bearing static eccentricity versus applied load when considering both a rigid pivot and a flexible pivot. As the static load increases, the journal eccentricity increases. At a given static load, the journal eccentricity given a flexible pivot is larger than the eccentricity given a rigid pivot. This is because at a particular static load, the film thickness on a pad remains the same whether the pivot is flexible or rigid thus ensuring that the static load remains the same. If the pivot is flexible, the pad displaces radially, allowing the journal to displace. For a flexible pivot, the radial pad displacement increases with increasing static load, hence the difference between the journal eccentricity of a rigid pivot and a flexible pivot increases as the static load increases.

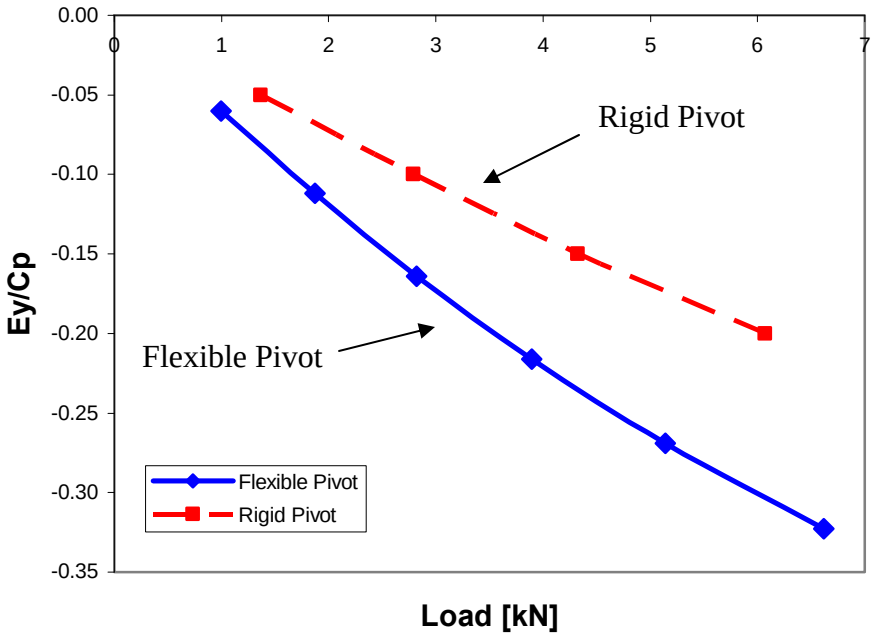

Figure 13: Predicted bearing static eccentricity versus static load (-*Y* direction)

Some observations

At a given load, journal eccentricity for a flexible pivot is larger than journal eccentricity for a rigid pivot bearing. Pivot flexibility decreases the direct static stiffness coefficients, a ~33% difference is noted between direct static stiffnesses of a flexible pivot and a rigid pivot bearings

Future work

Further work will be conducted to perform extensive comparisons between predicted force coefficients and Childs et al. [1,12-14] test data.

References [20-24] note that for a spherical pivot tilting pad bearing, **the pad slides about the pivot instead of rotating about a point (rolling without slipping).** References [20,22,24] find that as the pad slides about the pivot, friction impedes the tilting motion of the pad, thus affecting the journal eccentricities and increasing cross-coupled stiffness. Future work will be performed to account for the sliding motion and friction of a spherical pivot.

References [20,22] also note that for a rocker pivot, cross-coupled stiffnesses are small and journal eccentricities are well predicted when assuming the pad rotates about a line contact.

Literature Review (written by Jared Wilson, edited by Luis San Andres)

Lund (1964) [4] presented one of the first computational models predicting tilting pad bearing force coefficients. Even though predicted bearing force coefficients differ from experimental force coefficients obtained by Hagg and Sankey [5], Lund sets the foundation for modeling tilting pad bearing force coefficients. Sine Lund's original work, improved bearing models have followed that account for fluid inertia and turbulence flow effects, mechanical energy dissipation and heat transfer, and elastic deformation of the bearing pads, for example. Pad pivot stiffness has also been included in predictive models to bring about agreement with test data [6-9].

A review follows on the advances in modeling tilting pad bearing stiffness and damping force coefficients and the importance of pivot stiffness on the bearing dynamic force coefficients.

Lund [4] presents a comparison between predicted force coefficients and test results obtained by Hagg and Sankey [5] for a six pad, 50 degree arc tilting pad bearing. Figure 2 depicts the coordinate system and a representation of the bearing stiffness and damping coefficients as mechanical springs and dashpots. The bearing stiffness K and damping C coefficients include both direct (XX, YY) and cross-coupled (XY, YX) components.

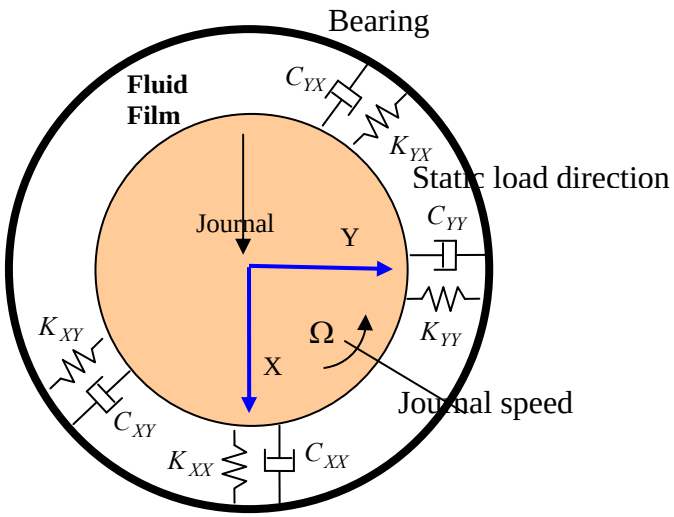

Figure 2: Conceptual depiction of stiffness and damping coefficients in a fluid film journal bearing

With the applied static load along the X direction, Ref. [4] shows predictions of direct stiffnesses (K_{XX}, K_{YY}) decreasing with increasing Sommerfeld[1] numbers (S). Predicted K_{XX} is consistently about three times larger than K_{YY}, but experimental results show that K_{XX} becomes larger than K_{YY} as S decreases, with K_{XX} about twice as large as K_{YY} at S~ 0.1. At a low Sommerfeld number[2] of 0.1, the predicted direct stiffness K_{YY} is similar to the experimental K_{YY}; however, the predicted K_{XX} is larger than the experimental K_{XX}. At a higher Sommerfeld number[3] of 3, the experimental K_{YY} is substantially under predicted with the experimental K_{XX} slightly under predicted. Comparison between theoretical and experimental damping shows that experimental direct damping C_{XX} is substantially over predicted at a low S~ 0.1; while at a high S=3, the experimental direct damping coefficient is predicted fairly well. Experimental direct damping C_{YY} is slightly over predicted at a low Sommerfeld number of 0.1; however, as S increases, C_{YY} is increasingly under predicted. Lund's bearing model does not account for flexibility in the pad pivot. **In actuality, the pivot stiffness is in series with the fluid film stiffness, hence affecting the bearing pad overall stiffness and damping coefficients.**

Later, in 1988, Someya [10] publishes experimental force coefficients for a five pad (LOP) tilting pad bearing. A static load in the X direction is applied on the bearing, as shown in Figure 2. Predictions of the direct stiffnesses (K_{XX}, K_{YY}) versus increasing Sommerfeld numbers (S) show a decreasing trend while the experimental results show an increasing trend. Thus, experimental direct stiffness coefficients at low S (high bearing loads) are over predicted and at high S (low bearing loads) are under predicted. Predicted damping coefficients (C_{XX}, C_{YY}) increase with increasing S, as the experimental direct damping coefficients also do. At low S, experimental direct damping coefficients are over predicted by a factor of three, but at S~ 0.5 they are only over predicted by 5% to 10%. This signifies that experimental damping coefficients become more over predicted as the bearing load increases, similar to the results in Ref. [4]. **Someya does not consider pivot stiffness in the analytical model, and as a result, bearing stiffness and damping coefficient are over predicted at high loads.**

Over a decade after Lund's analysis, Rouch [6] observes that the behavior of pivoted-pad bearings can be significantly affected by the flexibility of pad pivots, especially in large, heavily loaded bearings. To account for pivot flexibility, pad translation in the radial direction is included in the bearing analysis. Using a typical five pad bearing, Rouch shows the effects of pivot stiffness on the bearing frequency reduced (pads move with the same frequency as the shaft rotational speed) force coefficients for operation at three

---

[1] The Sommerfeld number is a non-dimensional number relating bearing static performance characteristics and is written as $S = \dfrac{\mu NLD}{W}\left(\dfrac{R}{C_P}\right)^2$ where μ =fluid viscosity, N=shaft speed(rev/s), L=pad length, D=bearing diameter, R=bearing radius, C_P =pad clearance, and W=applied load

[2] Large bearing loads, or low shaft speeds, or light lubricant viscosity, or large journal eccentricity

[3] Low bearing loads, or high shaft speeds, or large lubricant viscosity, or small journal eccentricity

shaft speeds. In the analysis, all pads have the same pivot stiffness, but it is noted that in actuality, **pivot stiffness is a function of the static load acting on each pad,** hence each pad has a different pivot stiffness. Rouch applies a static load in the Y direction, see Figure 2, and determines how pivot stiffness affects the bearing dynamic force coefficients. Direct damping coefficients (C_{XX}, C_{YY}) increase rapidly with an increase in pivot stiffness and then level out at a pivot stiffness over 10^{10} N/m. The bearing direct stiffnesses (K_{XX}, K_{YY}) increase with increasing pivot stiffness, leveling off at a pivot stiffness higher than 10^{10} N/m. The cross-coupled stiffness K_{YX} decreases with increasing pivot stiffness and goes to zero around a pivot stiffness between 10^8 and 10^9 N/m, and then increases until leveling off at a pivot stiffness over 10^{10} N/m. Rouch also varies pivot stiffness to determine how it affects rotor stability. He finds that **for large rotors, pivot stiffness and corresponding foundation flexibility can be significant factors in determining the stability of the rotor.**

In 1988, Kirk and Reedy [7] review Hertzian contact stress analysis in an effort to improve tilting pad bearing pivot designs. **Typical pivot designs range from line contact applicable to a rocker tilting pad bearing, to a point contact found in a ball-in-socket bearings.** The analysis considers an ideal line or point contact and negligible resistance to pad rotational motion. The calculation of pivot stiffness is based upon the results of Hertzian contact stress as given by Roark [11]. Using Hertzian contact stress formulas, pivot stiffness is a function of its material properties, contact area, and applied load. Kirk and Reedy report stiffness equations for pivot designs of a sphere contacting a flat plate, a sphere contacting a sphere, a sphere inside a cylinder, and a line contact pivot. Comparing predicted synchronous speed bearing stiffness coefficients with and without pivot stiffness over a range of shaft speeds, Ref. [7] notes that pad pivots representing a line contact and a point contact pivot behave similarly. For these cases, when pivot stiffness is considered, both synchronous speed reduced bearing damping and stiffness coefficients decrease. Kirk and Reedy also present the percentage differences between calculated pivot stiffness using the Hertzian approximation and a more exact general solution with pad pivot curvature effects. The authors find there is only a small difference between calculated pivot stiffness using the Hertzian approach and the exact solution. **Ref. [7] concludes that pivot flexibility can reduce the bearing damping coefficients, synchronous speed reduced, by as much as 72% if small radii spherical pivots are used.**

In 1990, Brockwell et al. [8] present predicted and experimental stiffness and damping force coefficients of a five pad, rocker tilting pad bearing for shaft speeds of 15, 30, 45, and 60 Hz over a bearing load range of 1.7 to 4.5 kN. The analysis considers pivot stiffness as a function of load using the line contact pivot stiffness equation in Ref. [7]. Brockwell et al. present the bearing direct stiffness coefficients (K_{XX}, K_{YY}) and direct damping coefficients (C_{XX}, C_{YY}) versus applied static load in the Y direction, see Fig. 2. The authors find the trend of predicted and experimental force coefficients versus load to be similar. Ref. [8] includes a comparison of predicted bearing direct damping coefficients using a pad rigid pivot and a pad flexible or elastic pivot. Predicted direct damping coefficient derived using a pad flexible pivot compare fairly well with the

experimental values as the bearing load increases; while the direct damping coefficients derived using a pad rigid pivot increasingly over predict experimental coefficients as the bearing load increases. Taking into account the pad pivot flexibility leads to a significant improvement in predicting the damping coefficients at high loads, in particular. However, in general, the force coefficients are still over predicted. Brockwell et al. attribute this over prediction in part to noise associated with signals from the displacement transducers.

In 1995, Kim et al. [3] analyze the dynamic force characteristics of a tilting pad journal bearing similar to that in Ref. [8]. The analysis considers cross film variable viscosity, heat transfer effects in the lubricant flow, pad elastic deformation, heat conduction effects in the pads, and elastic deformation effects in the pivot. Modal deflection modes are used to approximate the deformation of the pads top surface. Using the same bearing characteristics and load and frequency range, Kim et al. compare predicted synchronously reduced bearing stiffness and damping force coefficients with the experimental and analytical results reported by Brockwell et al. [8]. At shaft speeds of 30 and 45 Hz, Kim et al. predict direct stiffnesses (K_{XX}, K_{YY}) which correlate very well with the experimental coefficients. The predicted direct damping coefficients (C_{XX}, C_{YY}) match the experimental coefficients better than in Ref. [8] predictions, but a slight divergence between predicted and experimental values appears at high bearing loads.

In 1994, Chen [9] presents a general method for calculation of the dynamic force coefficients in tilting pad journal bearings. Flexibility of the tilting pad pivot in the radial, transverse, and rotational directions is taken into account. The analysis also models, at that time, the newly developed flexure-pivot tilting pad bearing. The pad is taken as a lumped inertia on the free end of a slender cantilever beam, and whose stiffnesses are found from simple bending formulas. For a five pad (LBP) flexure picot bearing, Chen compares predicted and experimental stiffness and damping force coefficients for a rigid pivot and a flexible pivot with load dependent pivot stiffness. Modeling with the flexible pivot, damping coefficients decrease by ~ 8% and stiffness coefficients by ~ 3% as compared to the coefficients obtained assuming a rigid pivot. Comparing a flexure-pivot with a line in contact pivot configuration, the damping coefficients are found to be lower for the flexure-pivot while the cross-coupled coefficients that result from the transverse resilience of the support web increase.

Al-Ghasem and Childs [12] present experimental rotordynamic coefficients for a four pad LBP) flexure pivot tilting pad bearing (FPB)[4]. The bulk flow model by San Andrés [2] is used to predict the static and dynamic forced performance of the FPB. The model takes into account pivot rotational stiffness, but neglects pivot deflection along the pad radial and transverse directions. Predicted direct stiffness coefficients (K_{XX}, K_{YY}) versus applied load show a trend similar to the experimental ones. However, predicted direct stiffnesses are larger than experimental ones, most noticeably at large static loads. Predicted K_{XX} at an applied load of ~ 9 kN and shaft speed of 8 krpm shows the largest

[4] Childs *et al.* static load is applied on the bearing in the $-Y$ direction as per Figure 2.

over prediction, and differs from experimental K_{XX} by ~ 35%[5]. Direct damping coefficients (C_{XX}, C_{YY}) increase with increasing static load, but decrease with increasing shaft speed. Direct damping coefficients are reasonably well predicted for low loads (~1.6 kN), but at high loads (~9 kN) these coefficients are over predicted significantly. Predicted C_{XX} at an applied load of ~ 9 kN and shaft speed of 8 krpm shows the largest over prediction, and differs from experimental C_{XX} by ~ 35%[6]. Refs. [6-9] note that at high loads, bearing direct damping and stiffness force coefficients reduce when pivot flexibility is considered. Thus, predicted direct damping and stiffness force coefficients would improve if radial pivot stiffness was considered in San Andrés [2] model.

In 2008, Hensley and Childs [13] tested at higher loads the same flexure pivot tilting pad bearing in Ref. [12]. Experimental force coefficients are found for applied loads ranging from ~ 9 kN to 19.5 kN, and shaft speeds between 6 to 12 krpm. It is important to note that the bearing clearance is slightly larger than that reported in Ref [12]; therefore stiffness and damping force coefficients at corresponding static loads in Ref. [13] are slightly lower than those in Ref. [12]. Hensley and Childs present experimental direct stiffness and damping coefficients versus increasing static load. Predicted direct stiffnesses are higher than experimental direct stiffness coefficients, most noticeably at the highest load. Predicted K_{XX} at an applied load of 17 kN and shaft speed of 8 krpm shows the largest over prediction, and differs from experimental K_{XX} by ~ 53%. Similarly, predicted direct damping coefficients are higher than experimental direct damping coefficients, again most noticeably at the highest applied load. Predicted C_{XX} at an applied load of 17 kN and shaft speed of 8 krpm shows the largest over prediction, differing from experimental C_{XX} by ~ 68%.

Carter and Childs [14] report rotordynamic force coefficients for a 5-pad, rocker-pivot, tilting pad bearing in a LBP configuration. Using a similar test setup as in Ref. [12], experimental bearing force coefficients are obtained over load ranges from ~ 2 N to 19 kN, and shaft speed ranges from 4 to 13 krpm. Using San Andrés [2] bulk flow model, predictions are made for the experimental direct stiffness (K_{XX}, K_{YY}) and direct damping (C_{XX}, C_{YY}) force coefficients. Both predicted and experimental direct stiffness coefficients increase with increasing static load and increasing shaft speed. However, unlike in Refs. [1,3], K_{YY} is under predicted while K_{XX} is over predicted. The most significant difference between predicted and experimental direct stiffness coefficients is seen at an applied load of ~ 19 kN and a shaft speed of 10 krpm, with a ~ 12% difference for K_{YY} and a ~ 30% difference for K_{XX}. Measured direct damping coefficients are almost completely insensitive to changes in static load. Direct damping force coefficients

---

[5]The percent difference equals $\%\_diff = \frac{K_P - K_E}{K_E}$, where K_P and K_E are the predicted stiffness coefficient and experimental stiffness coefficients, respectively.

[6] The percent difference equals $\%\_diff = \frac{C_P - C_E}{C_E}$, where C_P and C_E are the predicted damping coefficient and experimental damping coefficients, respectively.

(C_{XX}, C_{YY}) are over predicted and become increasingly over predicted with increasing static loads. The largest difference seen is between predicted and experimental C_{YY} at a static load of ~ 19 kN and a shaft speed of 10k rpm, with predicted C_{YY} ~ 50% larger than experimental C_{YY}. Again a reoccurring trend is noticed between predicted and experimental force coefficients. As the applied static load increases, the difference between predicted and experimental force coefficients increases.

In 2008, Harris and Childs [1] report experimental static performance characteristics and rotordynamic coefficients for a four pad, ball-in-socket, tilting pad journal bearing. Also included are predictions of journal static eccentricity, bearing power loss, oil outlet temperature rise, and rotordynamic force coefficients derived from the bulk flow model in Ref. [2]. By applying a static load to the bearing housing and measuring the relative displacement between the bearing housing and the rotor, a nearly uniform pad pivot stiffness $K_p = 354\,{}^{MN}/_{m}$ is found as the slope of the applied load versus recorded displacement. The pivot stiffness is expected to increase as the applied load increases, however this was not the case experimentally. The measured deflection accounts for the stiffness of the pad babbitt, the pad itself, the pivot, the pivot shim, and the bearing housing. The recorded stiffness measurements are lower than the pivot stiffnesses calculated using Kirk and Reedy [7] spherical pivot stiffness equation.

With regard to the rotordynamic force coefficients in Ref. [1], direct stiffness coefficients K_{XX} and K_{YY} are significantly over predicted, and the disagreement worsens as shaft speed increases. At a shaft speed of 12 krpm and a high static load of ~ 19.5 kN, a unit load[7] of ~ 1896 kPa, predicted direct stiffness coefficients are much larger than experimental direct stiffness coefficients, with a percent difference of ~ 66%. However, Harris and Childs calculate equivalent stiffness and damping coefficients by combining fluid film flexibility with pivot flexibility for each pad. The equivalent stiffness and damping coefficients from each pad are assembled to obtain the equivalent coefficients for the entire tilting pad bearing. The equivalent bearing stiffness coefficients decrease, and surprisingly, under predict the experimental values. The coefficient difference is ~ 25% for a shaft speed of 12 krpm and an applied load of ~ 19.5 kN. It is also important to note that experimental direct stiffness coefficients do not increase as substantially with load as reported in Refs. [12,14], most likely due to the low measured stiffness value of the pad[8] and pivot. Experimental direct damping coefficients C_{XX} and C_{YY} are also significantly over predicted, with a percent difference of ~ 86% at a shaft speed of 12 krpm and an applied load of ~ 19.5 kN. Equivalent direct damping predictions, including the effect of pivot flexibility, under predict experimental direct damping coefficients with a difference of ~ 50%. It is clear from Harris and Childs [1] that the measured stiffness of a pad and pivot directly affects the overall bearing stiffness and damping force coefficient predictions.

---

[7] Unit load = ${}^{W}/_{LD}$ where W is the static load, L is the length of the bearing, and D is the diameter of the bearing

[8] Pad babbitt also contributes to the low measured stiffness magnitude

Summary of literature review

Lund [4] and Someya [5] present predictions of experimental rotordynamic force coefficients. Their theoretical force coefficients over predict experimental force coefficients at low Sommerfeld numbers (large loads). Rouch [6] finds analytically that bearing stiffness and damping coefficients increase dramatically with increasing pivot stiffness. Kirk and Reedy [7] report pad pivot stiffness as a function of load and material properties. Using pivot flexibility in their model, both Brockwell et al. [8] and Kim et al. [10] present a comparison of predicted to experimental stiffness and damping coefficients. Ref. [7] reports that accounting for pivot stiffness improves the dynamic force coefficient predictions, especially damping coefficients. Chen [9] presents bearing force coefficient predictions for a rocker and flexure pad tilting pad bearing. The analysis takes into account both radial and transverse displacement in the pivot. A comparison between rigid pivots and flexible pivots show that the model using flexible pivots reduces the bearing predicted stiffness and damping coefficients compared to the stiffness and damping coefficients found using a rigid pivot.

Childs and students, Refs. [1,12-14], present tilting pad bearing experimental stiffness and damping coefficients for increasing static loads and shaft speeds. Direct stiffness tends to increase with load and shaft speed for a flexure tilting pad bearing, Refs. [12,13], and rocker tilting pad bearing, Ref. [14]. The ball-in-socket tilting pad bearing, Ref. [1], also gives similar results, except that the direct stiffness coefficients do not increase as significantly with static load and shaft speed, as reported in Refs. [12,13,14]. For each test bearing, predictions of the direct stiffness coefficients are too large, most noticeably at a high static load. In all four test bearings, experimental direct damping coefficients remain relatively constant with an increasing static load and increasing shaft speed, a occurrence not predicted by the model. Overall, San Andrés [2] bulk flow model over predicts the experimental force coefficients, in particular at large static loads. An improvement in bearing force coefficient predictions is noted in Ref. [1] when pivot stiffness is placed in series with the bearing force coefficients derived from a rigid pivot model.

Including pivot stiffness as a function of load has shown to improve the predictions of bearing force coefficient, in particular damping coefficients, see Refs. [6-9].

References

[1] Harris, J., and Childs, D., 2008, "Static Performance Characteristics and Rotordynamic Coefficients for a Four-Pad Ball-In-Socket Tilting Pad Journal Bearing," ASME Paper No. GT2008-5063.

[2] San Andrés, L., 1996, "Turbulent Flow, Flexure-pivot Hybrid Bearings for Cryogenic Applications," ASME J. Tribol., **118**(1), pp. 190-200.

[3] Kim, J., Palazzolo, A., and Gadangi, R., 1995, "Dynamic Characteristics of TEHD Tilt Pad Journal Bearing Simulation Including Multiple Mode Pad Flexibility Model," ASME J. Vib. Acoustics, **117**, pp. 123-135.

[4] Lund, J. W., 1964, "Spring and Damping Coefficients for the Tilting-Pad Journal Bearing," ASLE Trans., **7**, 4, pp. 342-352.

[5] Hagg, A. C., and Sankey, G. O., 1958, "Some Dynamic Properties of Oil-Film Journal Bearings with Reference to the Unbalance Vibration of Rotors," ASME J. Appl. Mech., **25**, 141.

[6] Rouch, K. E., 1983, "Dynamics of Pivoted-Pad Journal Bearings, Including Pad Translation and Rotation Effects," ASLE Trans., **26**, 1, pp. 102-109.

[7] Kirk, R. G., and Reedy, S. W., 1988, "Evaluation of Pivot Stiffness for Typical Tilting-Pad Journal Bearing Designs," J. Vib., Acoustics, Stress, and Reliability in Design, **110**, pp. 165-171.

[8] Brockwell, K., Kleinbub, D., and Dmochowski, W., 1990, "Measurement and Calculation of the Dynamic Operating Characteristics of the Five Shoe, Tilting Pad Journal Bearing," STLE Tribol. Trans., 4, **33**, pp. 481-492.

[9] Chen, W. J., 1995, "Bearing Dynamic Coefficients of Flexible-Pad Journal Bearings," ASME J. Tribol., 2, **38**, pp. 253-260.

[10] Someya, T., 1988, *Journal-Bearing Databook*, Springer-Verlag, Berlin, pp. 227-229.

[11] Roark, R. J., and Young, W. C., 1975, *Formulas for Stress and Strain*, 5th ed., McGraw-Hill, Columbus, OH, pp. 650-655.

[12] Al-Ghasem, A. M. and Childs, D., 2006, "Rotordynamic Coefficients Measurements Versus Predictions for a High-Speed Flexure-Pivot Tilting-Pad Bearing (Load-Between-Pad Configuration)," ASME J. Eng. Gas Turbines Power, **128**, pp. 896-906.

[13] Hensley, J. E., and Childs, D., 2008, "Measurements Versus Predictions for the Static and Rotordynamic Characteristics of a Flexure Pivot-Pad Tilting Pad Bearing in an LBP Condition at Higher Unit Loads," ASME Paper No. GT2008-5066.

[14] Carter, R. C., and Childs, D., 2008, "Measurements Versus Predictions for the Rotordynamic Characteristics of a 5-Pad, Rocker-Pivot, Tilting-Pad Bearing in Load Between Pad Configuration," ASME Paper No. GT2008-5069.

[15] "Tilting Pad Journal Bearings," Rotech Engineering, http://www.rotechconsulting.com/bearings_sub2.htm, [accessed 10 April 2008]

[16] Zeidan, F.Y., 1992, "Developments in Fluid Film Bearing Technology," Turbomachinery International, **9**, pp. 24-31.

[17] San Andrés, L., 2006, "Hybrid Flexure Pivot-Tilting Pad Gas Bearings: Analysis and Experimental Validation," ASME J. Tribol., **128**(1), pp. 551-558.

[18] Delgado, A., San Andrés, L., and Justak, J., 2004, "Analysis of Performance and Rotordynamic Force Coefficients of Brush Seals with Reverse Rotation Ability," ASME Paper No. GT 2004-53614.

[19] "Mobil DTE Oil Named Series" Exxon Mobil Corporation, 2007, http://www.mobil.com, [accessed 21 May, 2008]

[20] Wygant, K. D., Flack, R. D., and Barrett, L. E., 1999, "Influence of Pad Pivot Friction on Tilting-Pad Journal Bearing Measurements-Part I: Steady Operating position", *Trib. Trans*, **42**, pp. 210-215.

[21] Wygant, K. D., Flack, R. D., and Barrett, L. E., 1999, "Influence of Pad Pivot Friction on Tilting-Pad Journal Bearing Measurements-Part II: Dynamic Coefficients", *Trib. Trans.*, **42**, pp. 250-256.

[22] Pettinato, B., De Choudhury, P., 1999, "Test Results of Key and Spherical Pivot Five-Shoe Tilt Pad Journal Bearings-Part I: Performance Measurements," *Trib. Trans.*, **42**, 3, pp. 541-547.

[23] Pettinato, B., De Choudhury, P., 1999, "Test Results of Key and Spherical Pivot Five-Shoe Tilt Pad Journal Bearings-Part II: Dynamic Measurements," *Trib. Trans.*, **42**, 3, pp. 675-680.

[24] Brechting, B., Flack, R., Cloud, H. and Barrett, L., 2005, "Influence of Journal Speed and Load on the Static Operating Characteristics of a Tilting-Pad Journal Bearing with Ball-and-Socket Pivots," *Trib. Trans*., **48**, pp. 283-288.

APPENDIX A

Fluid induced moment on pad

The fluid film moment differential about the pad pivot is found by taking the cross product of vector $\vec{r}$ with the differential force vector $d\vec{F}$, i.e.

$$d\vec{M} = \vec{r} \times d\vec{F} \tag{A.1}$$

Including the pad thickness (t), the vector $\vec{r}$ is, from Figure A.1,

$$\vec{r} = \left[\left(R \sin\beta \right) \vec{\eta} + \left(R\left[1 - \cos\beta\right] + t \right) \vec{\xi} \right] \tag{A.2}$$

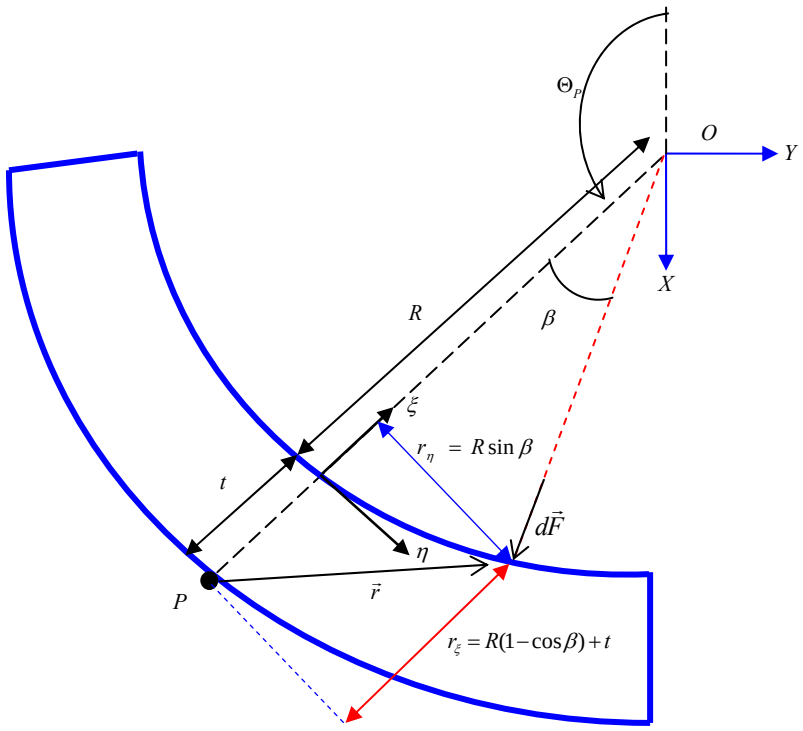

Figure A.1. Tilting pad with pivot point *P* and pad thickness *t*

The differential fluid film force vector can be written as

$$d\vec{F} = \left[dF_\eta \, \vec{\eta} + dF_\xi \, \vec{\xi} \right] \tag{A.3}$$

where $dF_\xi = -P\cos\beta \, R \, d\beta \, dz$ and $dF_\eta = P\sin\beta \, R \, d\beta \, dz$. The differential moment is thus

$$d\vec{M} = \left(-\left[R + t \right] P \sin\beta \right) R \, d\beta \, dz \, \vec{\kappa} \tag{A.4}$$

Expanding Eq. (A.4), using a trigonometry identity, and substituting in dF_η and dF_η, the differential fluid moment becomes

$$dM = \left[-\left(R+t\right)\left(-dF_Y \cos\Theta_P + dF_X \sin\Theta_P\right)\right] R \; d\theta \, dz \tag{A.5}$$

Integration over the pad surface gives the fluid moment M as

$$M = -\left(R+t\right)\left[- F_Y \cos\Theta_P + F_X \sin\Theta_P \right] \tag{A.6}$$

A change of coordinates results in the following transverse force equation:

$$F_\eta = -F_Y \cos\Theta_P + F_X \sin\Theta_P \tag{A.7}$$

Substituting equation (A.7) into (A.5) gives the following simpler version of the pad moment equation:

$$M = -(R+t)F_\eta \;=\; M = -R_P F_\eta , \tag{A.8}$$

with $R_p = R + t$

B. Derivation of Pad Mass Matrix

The pad mass matrix $[M_{pad}]$ is derived from the kinetic energy of a pad,

$$T_{pad} = \frac{1}{2} I_G \dot{\delta}^2 + \frac{1}{2} m (v_\xi^2 + v_\eta^2) \tag{A.9}$$

where I_G is a pad moment of inertia, and v_ξ and v_η are the pad velocity components in the radial and transverse directions, respectively. The pad center of mass translational velocities are

$$v_\xi = \frac{d}{dt}(d_\xi) = \frac{d}{dt}\left[-a - r(1-\cos\delta)\cos\alpha - r\sin\delta\sin\alpha - \xi \right] = -r\dot{\delta}\sin\delta\cos\alpha - r\dot{\delta}\cos\delta\sin\alpha - \dot{\xi}$$

$$v_\eta = \frac{d}{dt}(d_\eta) = \frac{d}{dt}\left[-b - r\sin\delta\cos\alpha + r(1-\cos\delta)\sin\alpha + \eta \right] = -r\dot{\delta}\cos\delta\cos\alpha + r\dot{\delta}\sin\delta\sin\alpha + \dot{\eta} \tag{A.10}$$

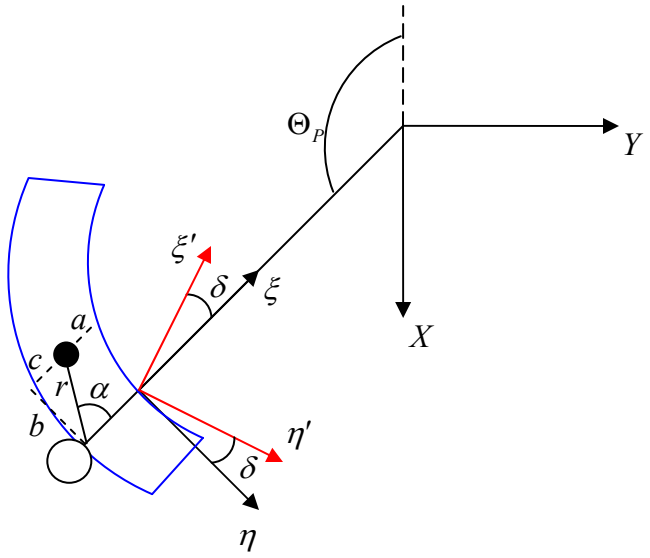

Figure A.2: Tilting pad with an offset pivot

Let b be the radial distance from the pad center of mass to the pad pivot, and c be the transverse distance from the pad center of mass to the pad pivot, see Figure 2. Substitute $\sin(\alpha) = \frac{b}{r}$ and $\cos(\alpha) = \frac{c}{r}$ into Eq. (A.10), and find v_ξ^2 and v_η^2 as

$$v_\xi^2 = \dot{\delta}^2 \sin^2(\delta)c^2 + 2\dot{\delta}^2 \sin(\delta)\cos(\delta)c*b + 2\dot{\delta}\dot{\xi}\sin(\delta)c + \dot{\delta}^2\cos^2(\delta)b^2 + 2\dot{\delta}\dot{\xi}\cos(\delta)b + \dot{\xi}^2$$

$$v_\eta^2 = \dot{\delta}^2 \cos^2(\delta)c^2 - 2\dot{\delta}^2 \sin(\delta)\cos(\delta)c*b - 2\dot{\delta}\dot{\eta}\cos(\delta)c + \dot{\delta}^2\sin^2(\delta)b^2 + 2\dot{\delta}\dot{\eta}\sin(\delta)b + \dot{\eta}^2 \qquad \text{(A.11)}$$

Substitute Eq. (A.11) into Eq. (A.9) and simplifying gives the following kinetic energy equation of the pad:

$$\begin{aligned} T_{pad} = {} & \frac{1}{2}I_G\dot{\delta}^2 + \frac{1}{2}m\dot{\delta}^2(c^2+b^2) + \frac{1}{2}m(\dot{\xi}^2+\dot{\eta}^2) \\ & + \sin(\delta)[m\dot{\xi}\dot{\delta}(c) + m\dot{\delta}\dot{\eta}(b)] \\ & + \cos(\delta)[-m\dot{\eta}\dot{\delta}(c) + m\dot{\delta}\dot{\xi}(b)] \end{aligned} \qquad \text{(A.12)}$$

The elements of the mass matrix $[M_{pad}]$ are derived from Eq. (A.12) using Lagrange's method for first order terms. Higher order terms are assumed to be ~zero, i.e., $\dot{\xi}\dot{\delta} \approx 0$, $\dot{\eta}\dot{\delta} \approx 0$, and $\dot{\delta}^2 \approx 0$.

$$\frac{d}{dt}\left(\frac{\partial T}{\partial \dot{\delta}}\right) = \left(I_G + m(c^2+b^2)\right)\ddot{\delta} + m\ddot{\xi}\sin(\delta)c - m\ddot{\eta}\cos(\delta)c + m\ddot{\xi}\cos(\delta)b + m\ddot{\eta}\sin(\delta)b$$

$$\frac{d}{dt}\left(\frac{\partial T}{\partial \dot{\xi}}\right) = m\ddot{\xi} + m\ddot{\delta}\sin(\delta)c + m\ddot{\delta}\cos(\delta)b \qquad \text{(A.13)}$$

$$\frac{d}{dt}\left(\frac{\partial T}{\partial \dot{\eta}}\right) = m\ddot{\eta} - m\ddot{\delta}\cos(\delta)c + m\ddot{\delta}\sin(\delta)b$$

Since the pad angle of rotation (δ) is very small, the assumption can be made that $\sin(\delta) \approx 0$ and $\cos(\delta) \approx 1$. The pad mass matrix is thus:

$$\left[M_{pad}\right] = \begin{bmatrix} I_P & m(b) & -m(c) \\ m(b) & m & 0 \\ -m(c) & 0 & m \end{bmatrix} \qquad \text{(A.14)}$$

with $I_P = I_G + m(c^2 + b^2)$ as the pad moment of inertia about the pivot.

.

NOMENCLATURE

A	Flexure pivot web cross sectional area [m^2]
a	Radial distance from pad mass center of gravity to pad surface [m]
b	Radial distance from pad mass center of gravity to pivot [m]
c	Transverse distance from pad mass center of gravity to pivot [m]
C_p	Journal bearing radial clearance
C_m	Assembled bearing radial clearance [m]
$[C^k]$	Tilting pad bearing pivot damping matrix [Ns/m]
$C_{R\alpha\beta}$	Bearing Reduced damping coefficients at frequency ω; $\alpha,\beta = X,Y$ [Ns/m]
D	Bearing diameter [m]
D_H	Pivot housing diameter [m]
D_P	Pivot diameter [m]
E	Young's Modulus of pivot and pivot housing [Pa]
e_X, e_Y	Journal eccentricity in the (X,Y) direction respectively
F_X^k, F_Y^k	Fluid film forces on pad along the {X,Y} axes [N]
$F_{P\xi}^k,\ F_{P\eta}^k$	Fluid film forces on pad along the $\{\xi,\eta\}$ axes [N]
F_ξ^k, F_η^k	Radial and transverse fluid film forces [N]
h	Fluid film thickness [m]
$h_o, \Delta h$	Equilibrium film thickness, perturbed film thickness [m]
I	Flexure pivot web area moment of inertia [m^4]
I_p^k	Pad moment of inertia at pivot [kgm^2]
$K_{R\alpha\beta}$	Bearing reduced stiffness coefficients; $\alpha,\beta = X,Y$ [N/m]
$[K^k]$	Tilting pad bearing pivot stiffness matrix [N/m]
L, L_R, L_L	Bearing axial length; $L = L_R + L_L$
L_{web}	Flexure pivot web length [m]
M_P^k	Moment from pivot rotational stiffness [N-m]
M^k	Fluid film moment on pad; $R\{\sin(\Theta_p^k)F_X^k - \cos(\Theta_p^k)F_Y^k\}$ [Nm]
$[M_{mass}^k]$	Pad mass matrix, includes pad inertia, angular momentum, and mass
m^k	Pad mass [kg]
N	Shaft rotational speed [rev/s]
P	Fluid film pressure [N/m^2]
$P_o, \Delta P$	Fluid film equilibrium pressure, Fluid film perturbed pressure [N/m^2]
R	Pad radius [m]
R_p	Pad radius plus pad thickness [m]
r_p	Pad preload [m]

S	Sommerfeld number, $S = \dfrac{\mu NLD}{W}\left(\dfrac{R}{C_p}\right)^2$
W	Applied static load [N]
$\{X,Y,Z\}$	Inertial coordinate system
$Z^k_{\alpha\beta}$	k^{th} pad impedance, $K^k_{\alpha\beta} + i\omega C^k_{\alpha\beta}$, $\alpha,\beta = X,Y,\delta,\xi,\eta$
δ^k	Pad rotational angle [rad]
η^k	Pad transverse displacement [m]
μ	Fluid viscosity [Ns/m^2]
υ	Poisson ratio of pivot and pivot housing
θ	Circumferential or angular coordinate, x/R
Θ^k, Θ^k_l	k^{th} pad angular length, k^{th} pad leading edge angular position [rad]
Θ_p	k^{th} pad pivot angular position [rad]
Ω, ω	Rotational speed of journal, excitation or whirl frequency [1/s]
ξ^k	Pad radial displacement [m]